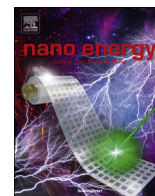




ELSEVIER

Contents lists available at ScienceDirect

Nano Energy

journal homepage: www.elsevier.com/locate/nanoen

All-flexible lithium ion battery based on thermally-etched porous carbon cloth anode and cathode



Muhammad-Sadeeq Balogun^a, Weitao Qiu^a, Feiyi Lyu^a, Yang Luo^a, Hui Meng^a, Jiantao Li^a, Wenjie Mai^{c,*}, Liqiang Mai^{b,*}, Yexiang Tong^{a,*}

^a MOE of the Key Laboratory of Bioinorganic and Synthetic Chemistry, KLGHEI of Environment and Energy Chemistry, The Key Lab of Low-carbon Chem & Energy Conservation of Guangdong Province, School of Chemistry and Chemical Engineering, Sun Yat-Sen University, Guangzhou 510275, PR China

^b State Key Laboratory of Advanced Technology for Materials Synthesis and Processing, Wuhan University of Technology, Wuhan 430070, PR China

^c Department of Physics and Siyuan Laboratory, Jinan University, Guangzhou 510632, PR China

ARTICLE INFO

Article history:

Received 5 March 2016

Received in revised form

5 May 2016

Accepted 10 May 2016

Available online 2 June 2016

Keywords:

Carbon cloth

Flexible

Lithium ion battery

Porous

Thermal-etching

ABSTRACT

Flexible electrode material with high mechanical strength and excellent electrical stability is still a great challenge for the fabrication of highly flexible energy storage devices. Commercial carbon cloth has been long reported as flexible substrate for many electrode materials due to their high mechanical strength and flexibility. However, their application directly as electrode material for flexible lithium ion batteries is yet to be reported. In this paper, commercial carbon cloth was thermally etched and used directly as electrode material in the half-cell and all-flexible full lithium ion batteries. Upon the mass weight and the large diameter of the carbon fiber, the as-prepared free-standing N-doped Porous carbon cloth delivered an initial capacity of 1.75 mA h/cm² (190 mA h/g) and capacity up to 1.65 mA h/cm² (168 mA h/g) after long electrochemical cycles in the half-cell. The all-flexible device exhibits a high working potential of 3.4 V, remarkable lithium storage performance and excellent flexibility. It also achieves a maximum volumetric energy density of 43 W h/cm³ at 0.125 mA/cm² and power density 800 W/cm³ at 5.0 mA/cm². The excellent performance can be attributed to N-doped porous surfaces, which provide large surface area for more lithium storage.

© 2016 Elsevier Ltd. All rights reserved.

1. Introduction

Searching for suitable flexible electrochemical storage devices (ESD) requires the development of flexible components such as flexible electrodes, separators and electrolytes [1–6]. To achieve a long term use flexible ESD, these flexible components should not affect power supply during electrochemical processes under frequent (different or different type of) deformation modes [7–9]. One of the key challenges to realize reasonable flexible ESDs is to design and fabricate reliable materials with high energy density, high power density, good cycling stability and robust flexibility [10,11]. For electrode materials, various flexible materials based on carbon nanotubes (CNTs) [12,13], graphene [14], carbon cloth [15,16] and conductive paper [17], with nanostructured materials and their composites [18,19] have been employed for the development of flexible ESDs due to their affordable production cost, outstanding electrical conductivity, and attractive electrochemical stability [20–22].

Among the various flexible electrode, carbon cloth commonly termed as CC, a highly conductive textile with more excellent mechanical flexibility and strength [23,24] than the graphene, CNTs and cellulose paper, holds a great commitment in serving as a flexible substrate in the fabrication of flexible ESD [25,26]. It could also act as the function of a three-dimensional (3D) current collector and flexible substrate for the preparation of various electrochemically active materials [27,28] to form composites [29] such as the metal oxides [30], nitrides [31], sulfides [32], metal-organic frameworks [33], and alloy materials composites [34,35]. According to X-ray diffraction pattern (Fig. 1a–I), CC is a kind of hard carbon with major peaks around 25.3° and 43.1° [36–38]. Based on the results given by different reports, CC usually delivered a specific capacity of approximately 20 mA h/g (0.15 mA h/cm²) at current density of about 1000 mA/g [39] or specific capacitance of 1–2 F/g at a scan rate of 100 mV/s [40], respectively, which justify that they grip a considerable potential as electrode material for common ESDs (Li-ion batteries and supercapacitors). However, the capacity/capacitance is relatively low compare to graphite (372 mA h/g), carbon nanosheets, graphene, carbon nanotubes because CC possess a small surface area due to the large diameter of each carbon fiber cloth (~5 μm) [40]. Thus,

* Corresponding authors.

E-mail addresses: wenjimai@gmail.com (W. Mai), mlq518@whut.edu.cn (L. Mai), chedhx@mail.sysu.edu.cn (Y. Tong).

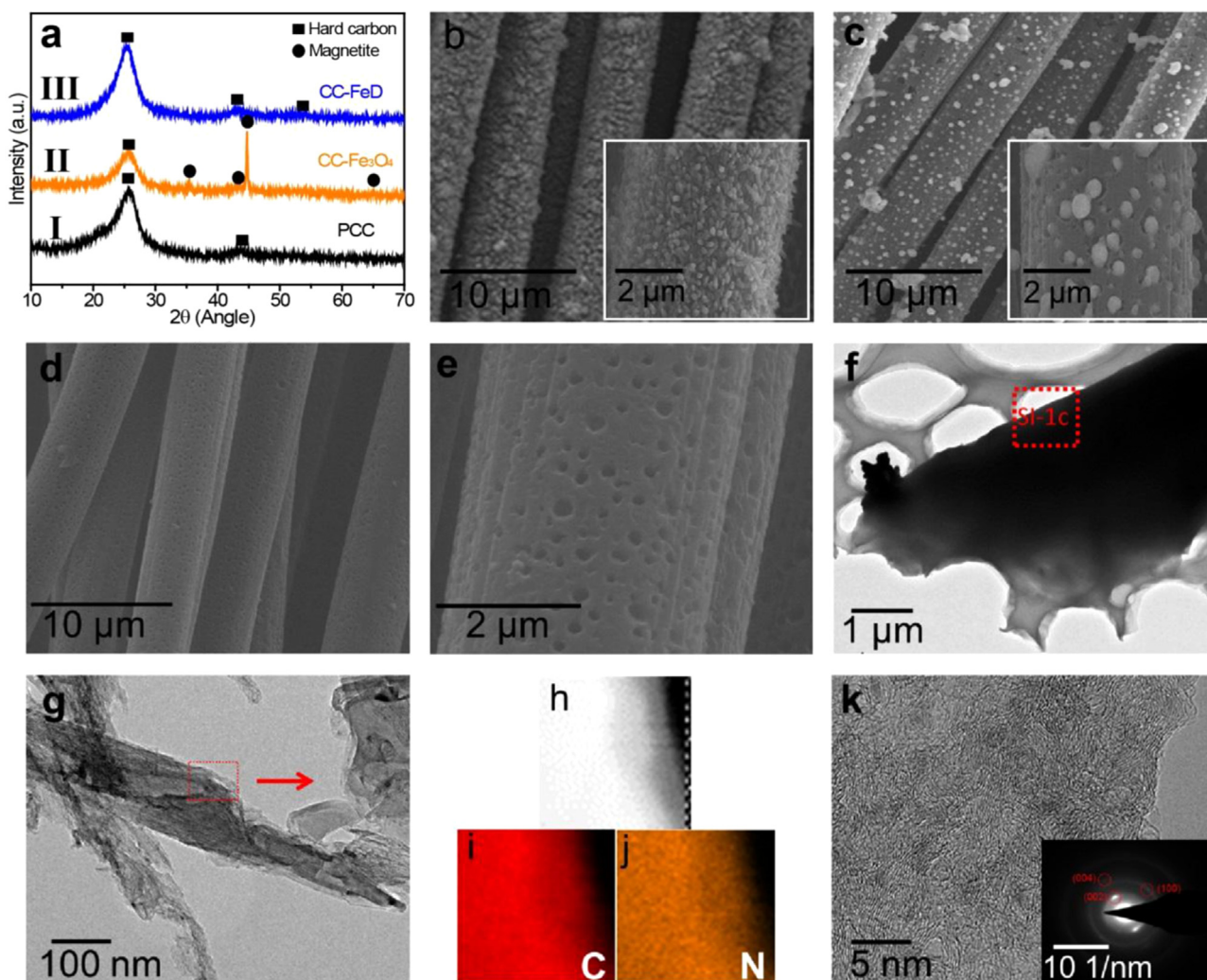


Fig. 1. (a) XRD pattern of the PCC, CC-Fe₃O₄ and CC-FeD samples. SEM images of (b) CC-FeOOH NRs (Inset is the low magnification image), (c) porous CC-Fe₃O₄ NPs (Inset is the low magnification image), (d) porous CC-FeD and (e) Enlarge SEM image of the CC-FeD). (f) TEM image of the PCC sample displaying the smooth surface of the carbon fiber. (g) TEM image of the CC-FeD sample displaying the rough surface of the carbon fiber. (h–j) EDS elemental mapping of the of the red-dazed area in "g" showing the distribution of the Carbon and Nitrogen. (k) HRTEM image of the CC-FeD sample identifying the porous exfoliated carbon fiber. Inset is the Corresponding SAED pattern of the CC-FeD.

they attracted less attention in terms of utilizing them directly as electrode material for ESDs. Lately, chemical and electrochemical activation approach have been employed to boost electrochemical capacitive properties of CC for supercapacitors [40–42], while no attempt has been made on enhancing the electrochemical performance of CC as lithium ion battery electrodes.

For Lithium ion batteries (LIB), most reported papers based on the electrochemically active materials been prepared on the surface of CC usually calculate the capacity contribution of the CC based on two methods; (i) The capacity obtained during lithium insertion below 0.4 V [43]. (ii) The percentage ratio of the CC specific capacity (mA h/cm²) to the whole electrode specific capacity in mA h/cm² (total mass of the active materials and CC in mg) [26,44]. Generally, the capacity contribution of the CC is often calculated to be around 9–20% and even become lower when the current density increases, which indicates that the chance to improve their capacity contribution or directly use them as anode material for LIBs is very broad.

Having this in mind, we demonstrated an effective strategy to remarkably improve the lithium storage properties of CC using an acid-treatment of thermally reduced metal oxide precursors (Fe and Co precursors) and demonstrate their application as electrode material for LIBs. A porous surface nitrogen-doped CC (denoted as CC-FeD) was obtained after the acid treatment of thermal etching.

This N-doping and porous surfaces made the modified CC suitable for storing more Li⁺. The CC-FeD electrode exhibited a discharge capacity of 0.661 mA h/cm² at a current density of 3720 mA/g, which is 44 times of the untreated CC. The CC-FeD sample was then used as a flexible substrate for casting of LiCoO₂ cathode (denoted as CC-LCO), which were used in the assembling the full coin and all-flexible LIBs. The CC-FeD//CC-LCO coin and all-flexible LIBs exhibit excellent lithium storage performance and remarkable flexibility. The all-flexible cell also delivered maximum energy and power density of 43 W h/cm³ and 800 W/cm³ at 0.125 mA/cm² and 5.0 mA/cm², respectively. This proves our porous carbon cloth could be potential and promising electrode material for high power density lithium ion batteries.

2. Experimental section

2.1. Synthesis of the CC-FeD sample

All reagents were of analytical grade and were directly used without any purification. CC (0.5 g, 12.6 mg/cm²) was purchased from Fuel Cell Earth. Firstly, FeOOH nanorods were grown on the CC (denoted as CC-FeOOH) as reported in our previous papers [45–47]. The CC-FeOOH was then annealed in N₂ atmosphere at 900 °C

for 1 h. The furnace was then allowed to cool to room temperature and CC-Fe₃O₄ samples were obtained. The CC-Fe₃O₄ sample were immersed in conc. HCl overnight to dissolved the magnetite NPs and porous CC-FeD were obtained.

2.2. Synthesis of the CC-CoD sample

Co precursor was first obtained on the CC by hydrothermal reaction according to Xia et al. with slight modification. In a typical synthesis, 6 mmol of Co(NO₃)₂·6H₂O, 12 mmol of NH₄F and 30 mmol of CO(NH₂)₂ were dissolved in 35 ml of distilled water under continuous stirring. The obtained homogenous solution was transferred into Teflon-lined stainless steel autoclaves with CC and heated at 120 °C for 6 h. After cooling down to room temperature, thermal reduction and acid treatment were then carried out as discussed above.

2.3. Characterization

The morphology, structure and composition of the electrode materials were characterized by field emission SEM (JSM-6330F) and transmission electron microscope (TEM) (JEM2010-HR, 200 KV). The element identification and heteroatom functional group distribution was measured through photoelectron spectroscopy (XPS, ESCALab250). The crystallographic information and phase purity of the products were characterized by X-ray diffraction Spectrometry (XRD; Shimadzu X-ray diffractometer 6000, Cu K α radiation, Shimadzu, Tokyo, Japan) and Raman Spectroscopy (Renishaw inVia).

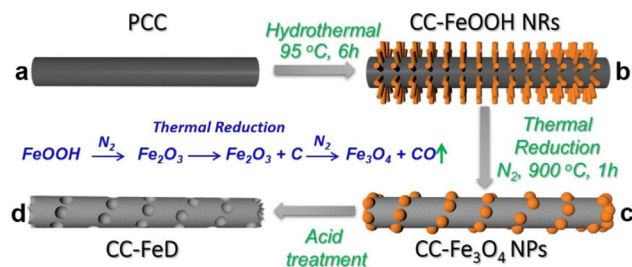
2.4. Electrochemical measurements

The binder free electrodes (PCC, CC-Fe₃O₄, CC-FeD and CC-CoD) were directly used as the anode, while the CC-FeD or CC-CoD flexible substrate coated with LCO was used as cathode. The PCC and modified CC samples were first cut into many smaller square pieces with 1.0 cm² area. The mass loadings of samples are approximately 10 mg/cm² measured by a Sartorius Analytical Balance (CPA225D, maximum weight 5100 mg with a resolution of 0.001 mg, Sartorius, Germany). For the cathode materials, the electrodes were fabricated by mixing the LCO powders and PVDF binder at weight ratios of 90:10. The slurry was then casted on the CC-FeD substrate, transferred to a vacuum oven and dried at 110 °C overnight. Half cells were assembled in a coin cell using 1 M LiPF₆ in ethylene carbonate (EC) and diethyl carbonate (DEC) [(1:1)] solution as the electrolyte, Celgard 2400 was used as the separator and Li foil as both counter and reference electrodes. The galvanostatic charge/discharge tests were carried out between 0.01–3.0 V for anode vs. Li/Li⁺ (at different C rates, 1 C=372 mA h/g), 3.0–4.3 V for cathode and 2.5–3.9 V for the full coin cell LIB on a Neware Battery Testing System (Shenzhen, China).

3. Results and discussion

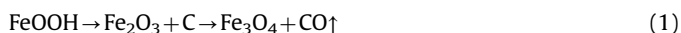
3.1. Fabrication process and morphology

N-doped Porous carbon cloth was prepared through a simple hydrothermal, followed by thermal reduction and acid-treatment according to the schematic process displayed in Scheme 1a-d. The Scanning electron microscopy (SEM) image of the bare CC can be seen in Fig. S1a of the Supporting Information. The SEM images show that the surface of the carbon cloth is smooth with a diameter and thickness of 5 and 7.5 μ m, respectively (Fig. S1a and S1b). Firstly, hydrothermal process was used to grow the FeOOH



Scheme 1. (a-d) Schematic illustration procedure of the N-doped porous CC-FeD sample.

films (CC-FeOOH NRs) on the CC (Scheme 1b) according to our previous report [46–48]. SEM image shows the uniform nanorod morphology of the FeOOH (Fig. 1b and S2a). Then, thermal reduction of the CC-FeOOH NRs by being annealed in N₂ environment results in the formation of CC-Fe₃O₄ nanoparticles (CC-Fe₃O₄ NPs) (Scheme 1c). At this stage the thermal reduction process enables the formation of porous CC surface with the NPs gluing to the CC inner portions, which can be confirmed by the SEM image in Fig. 1c inset. During the annealing process in N₂ atmosphere, the following reaction was proposed:



As displayed in Fig. 1a-II, the circle symbols are ascribed to the typical magnetite structure (JCPDF #19-0629). SEM image of the CC-Fe₃O₄ sample showed that uniform nanoparticles (NPs) were decorated in the inner and part of the CC (Fig. 1c) and the surface of the CC became roughen as well (Fig. S2b). Comparing the SEM image of the FeOOH NRs and Fe₃O₄ NPs, the mass loading of the as-grown film drastically reduces after thermal reduction in N₂ atmosphere. Weight loss of about 90% was calculated with 0.16 mg mass loading of Fe₃O₄ NPs on 1.0 cm² CC. Then the CC-Fe₃O₄ NPs was then subjected to acid treatment for the elimination of Fe₃O₄ NPs and achievement of high BET surface area with high total pore volume product, CC-FeD (Scheme 1d). SEM image in Fig. 1d affirmed that large amount of large-sized mesopores ~80–100 nm was formed after the dissolution of Fe₃O₄ NPs in conc. HCl, which are the pores of the CC-FeD sample (Fig. 1e). The enlarged images of Fig. 1d and e can be seen in Fig. S3 for further clarification. XRD measurement confirmed that the absence of magnetite NPs and the newly measured peaks correspond to the CC-FeD sample (Fig. 1a-III). The XRD pattern of the CC-FeD sample is the same with that of the pristine CC (PCC) but the peaks were much intensified affirming modification of the CC. ICP analysis carried out on the CC-FeD solution (solution obtained from further immersion in conc. HCl for 48 h) shows that there are no traces of any element confirming that the CC-FeD is purely carbon.

To gain further insight on the structure and morphology of the CC-FeD sample, transmission electron microscopy (TEM) analysis was performed. The TEM and High-resolution TEM (HRTEM) images of the pristine carbon cloth show that the surface and the inner part of the PCC are very smooth (Fig. 1f, S1c and S1d). The TEM analysis on the CC-FeD sample presented porous fibers (Fig. 1g). The HRTEM image collected at the edge of the porous fiber paraded exfoliated fibers (Fig. 1k) and further selected-area electron diffraction (SAED) pattern of the CC-FeD sample exhibited an amorphous nature with (002), (004) and (100) planes confirming the hard-carbon like of the CC-FeD (Fig. 1k inset). Energy dispersive X-ray spectroscopy (EDS) elemental mapping was collected from the CC-FeD exfoliated region (Fig. 1h). The result demonstrated that the sample mainly consist of carbon (Fig. 1i) and N (Fig. 1j) with uniform distribution of the N in the carbon matrix. It also reveals that the CC-FeD has C:N ratio of 99:1, which confirmed the doping of N in the CC-FeD sample. Further discussion

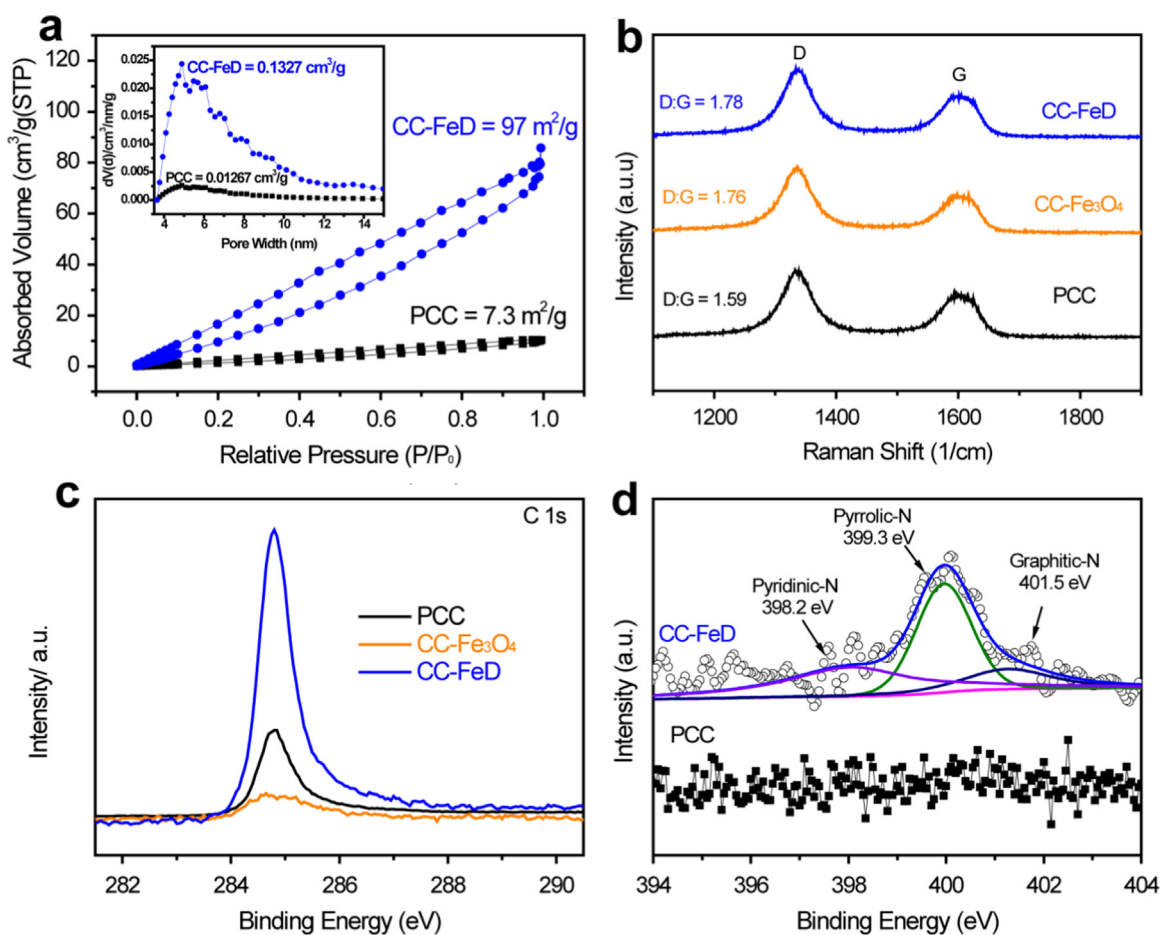


Fig. 2. (a) Nitrogen adsorption isotherms of PCC and CC-FeD at 77 K where STP stands for standard temperature and pressure conditions. Inset: Pore-width distribution of untreated and activated CC. (b) Raman spectra of the PCC, CC-Fe₃O₄ and CC-FeD samples showing the ratio of D:G. (c) C 1s XPS spectra of the PCC, CC-Fe₃O₄ and CC-FeD samples identifying the intensity of the CC-FeD sample carbon peak. (d) N 1s XPS spectra of the PCC and CC-FeD sample.

and justification of the N-doping can be seen in the XPS spectra analyses.

3.2. Characterization of the electrodes

Our approach to increase the capacity of the CC involves increasing its surface area via thermal reduction of the Fe(III) in N₂ atmosphere to obtain porous exfoliated CC. Thus, we carried out Brunauer-Emmett-Teller (BET) measurements on PCC and CC-FeD to derive comprehensive quantitative data on the enhanced surface area of the CC-FeD sample after modification. Fig. 2a depicted the N₂-absorption isotherms and pore-width distribution of PCC and CC-FeD. As expected, the surface area of the CC-FeD is 97 m²/g (0.1327 cm³/g pore volume), which is 14 times higher than that of the PCC at 7.3 m²/g (0.01267 cm³/g pore volume). With such enhancement in the surface area, we expect rapid diffusion of Li-ion in the CC-FeD sample, which could significantly boost its lithium storage capacity and rate performance over the PCC sample. Raman spectroscopy carried out shows that there were no obvious differences in the D and G band of the three samples. However, the intensity ratio of the D:G still emerge some slight differences (Fig. 2b). The D:G peak intensity ratio of the PCC sample is 1.59, which is lower than that of the CC-Fe₃O₄ (1.71) and CC-FeD (1.78). Such results affirmed the surface modification of the CC.

Furthermore, the X-ray Photoelectron Spectroscopy analysis provides more information on the composition of the samples. The XPS survey spectra of the CC-FeD sample displayed a highly-intensity C 1s peak and N 1s peak (Fig. S4a). Fig. 2c displayed the C 1s

XPS spectra of the samples, which identified that the C 1s peak of the CC-FeD sample exhibited highest intensity also confirmed the successful modification of the CC. Note that there are no additional peaks of the carbon in the C 1s XPS spectra of the sample because our modified CC sample was not subjected to oxidation but strictly thermal reduction and acid-treatment, which could not affect its structure. Moreover, during thermal reduction, nitrogen heteroatom was doped on the surface of the modified CC. The presence of heteroatoms at the surface of carbon-based materials has been reported to significantly enhance the kinetics of an electrode, thus attracting more Li ion storage capacity [49–51]. Herein, Fig. 2d shows the high resolution N1s XPS spectra of the PCC and CC-FeD samples. While no traces of N in the PCC sample, the CC-FeD reveals peaks centered at 398.2, 399.3 and 401.5 eV corresponding to hexagonal pyridinic-N, pyrrolic-N and graphitic-N, respectively, which can be fitted to three different types of doped N [52,53]. The N-doping are formed predominately through substitution of N on edges or defect sites with a carbon atom in the porous carbon cloth system or plane. These made the carbon atoms chemically more active than the untreated carbon cloth. Such N-doping in the carbon cloth can enhance the electrochemical reactivity and electronic conductivity [50–53], which additionally can also contribute to the excellent storage performance.

Furthermore, Fe 2p core-level spectra collected for the CC-FeD sample also confirmed no traces of Fe compared to that of CC-Fe₃O₄ (Fig. S4b), likewise the O 1s core-level spectra of the CC-FeD is almost the same with that of PCC (Fig. S4c), further affirming that our as-prepared CC-FeD mainly consist of carbon. All

these results are consistent with one another and compromise that the CC already undergoes modification. With these treatments, we expect that our as-prepared CC-FeD electrode will exhibit exceptional electrochemical performance over the untreated CC (PCC).

3.3. Lithium storage properties of the CC-FeD anode

The electrochemical performance of the electrodes was studied in a half coin-cell configuration with Li foil as the reference and counter electrodes. For effective comparison, we first investigated the effect of N_2 treatment on the PCC. The PCC was annealed in N_2 atmosphere at the 900 °C for 60 min to obtain the NCC sample. XRD and Raman spectra show that there were no obvious phase changes between the PCC and NCC after thermal treatment (Fig. S5). The NCC shows higher capacity than the PCC at very a low current density (0.5 C). This indicates that the N_2 treatment has slight effect on the lithium storage performance of the bare CC. (Fig. S6) However, the two electrodes displayed almost the same electrochemical properties beyond 0.5 C (Fig. S6). Thus, further electrochemical measurements were carried out on the PCC and CC-FeD electrodes.

Fig. 3a shows the first cyclic voltammetry (CV) curves collected for PCC and CC-FeD electrodes at a scan rate of 0.1 mV/s. Firstly,

both electrodes show a cathodic peak at 0.68 and 0.62 V, respectively, which are common characteristic cathodic peak of the hard carbon during the first discharge process [50,54]. During the second cycle, both electrodes show excellent reversibility with the initial reduction peaks at 0.68 and 0.62 V shifting to 0.91 and 0.86 V for the PCC and CC-FeD electrodes, respectively (Fig. S7). The reduction peaks at 0.12 V appear in the second and continuous cycles due to the reversible insertion of Li-ions into the CC cavities [55]. It should be pointed out that the 0.12 V reduction peak is more subtle in the CC-FeD than the PCC electrode justifying more lithium insertion in the CC-FeD electrode. Secondly, the CC-FeD electrode displayed an increased area of the CV curves when compare with the PCC. This suggests enhanced rapid Li insertion ability of the CC-FeD electrodes and such increased area is continuous in the following cycles (Fig. S7a and S9a). Meanwhile, the CV curve of the CC-Fe₃O₄ shows much larger area due to the contribution from the magnetite NPs and the redox peaks associated with magnetite and carbon can be observed (Fig. S10). In general, it can be apparently observed in the CV curves that the N-doping and pores introduction on the CC surface distinctly improved the electrochemical reactivity of the reactions. These factors are expected to enhance the capacity of the modified CC. Undoubtedly, the charge-discharge profiles in Fig. 3b affirmed the

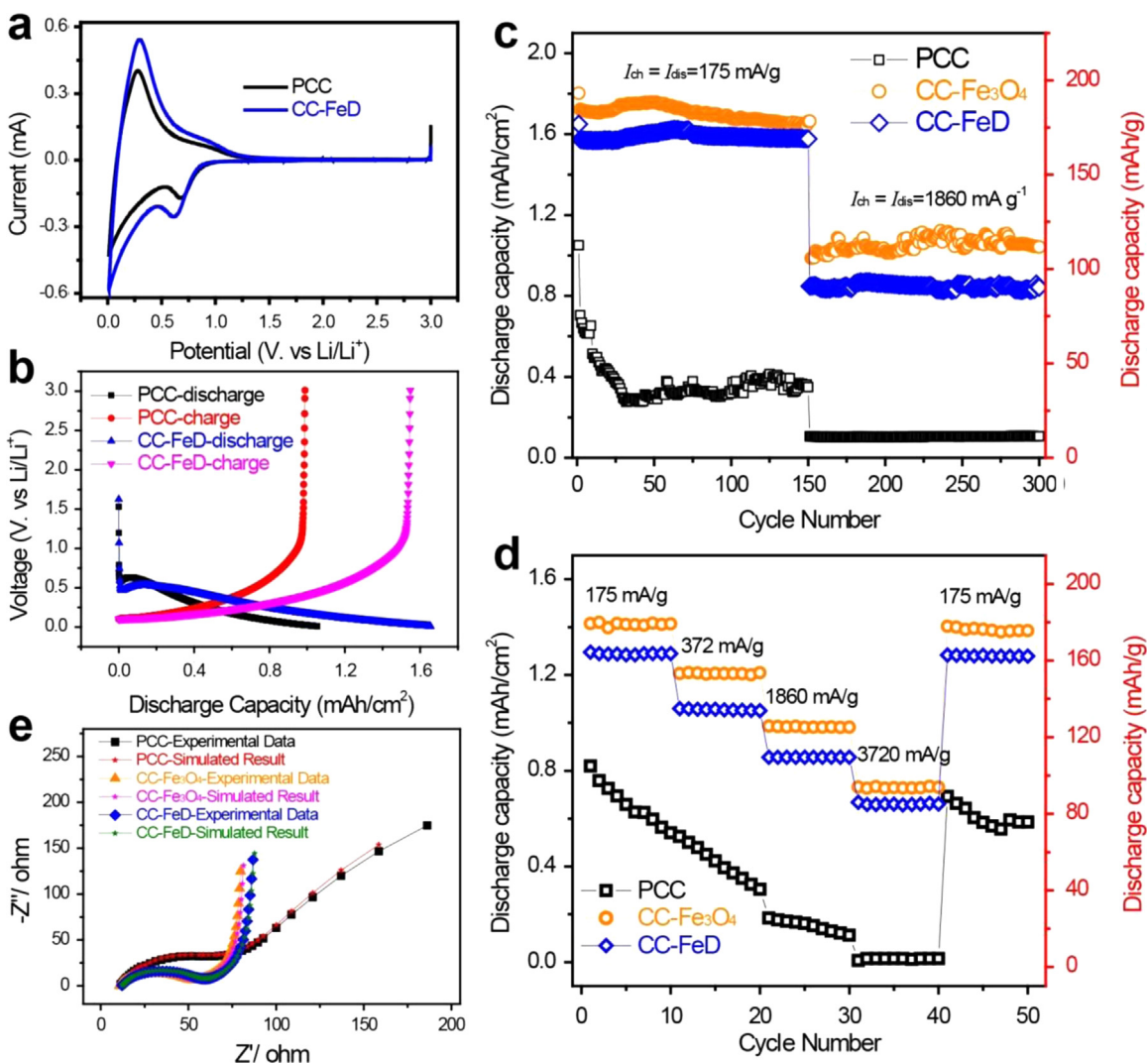


Fig. 3. Lithium storage performance of the electrodes. (a) CV profiles of the PCC and CC-FeD electrodes. (b) Discharge-charge profiles of the PCC and CC-FeD electrodes. (c) Cyclic stability at current densities of 175 and 1860 mA/g, (d) Rate capability test at increasing current densities and (e) Nyquist plot of the PCC, CC-Fe₃O₄ and CC-FeD electrodes. Inset in e is the equivalent circuit.

capacity enhancement of the CC-FeD electrode. A discharge plateau around 0.65 V is noticed in both electrodes, which is consistent with the result obtained from the CV test. The first discharge and charge capacity of the CC-FeD electrode at a current density of 175 mA/g is 1.69 mA h/cm² (190 mA h/g) and 1.59 mA h/cm² (178 mA h/g) respectively and higher than that of the PCC electrode (1.05 and 0.95 mA h/cm²). 94% initial coulombic efficiency was delivered by the CC-FeD electrode, reaching 100% after subsequent cycles (Fig. S11) and a continuous superior lithium storage ability over the PCC can also be observed in the subsequent cycles (Fig. S7b, S8 and S9b). Generally, hard carbon generally has very high irreversible capacity in the first cycle but seems very low in this report. Considering the thickness and the diameter of the carbon cloth that is about 5 μm, it is quite difficult for lithium to intercalate, which will surely leads to low irreversible capacity. Moreover, the commercial carbon cloth have low capacity (20 mA h/g) and our strategy is to improve its capacity, which we successfully achieved in this work. Furthermore, the mass loading of the carbon cloth per cm² reaches 10 mg. Such high mass loading is expected to display low irreversible capacity compare to the commonly reported hard carbon.

Studies on the cycle stability of the electrodes were carried out at 175 and 1860 mA/g current densities up to 150 cycles for each current density. Fig. 3c shows the extremely high cyclic stability of the electrodes. For comparison, the CC-Fe₃O₄ was also cycled. During the first seventieth cycling, the capacity of the composite electrode displayed a frivolous increment. At the end of the 1st and 2nd 150 cycles at 175 and 1860 mA/g current densities, the capacity retained by the CC-FeD electrode is 1.57 and 0.84 mA h/cm², respectively. These capacities are 4 and 20 folds higher than the PCC electrodes (0.35 and 0.09 mA h/cm²) at 175 and 1860 mA/g current densities, respectively. These values are even higher than some of the metal oxide based electrode calculated in areal capacity such as the 3D Ni/TiO₂ nanowire [56], SnO₂/Fe₂O₃ composite [57], TiO₂/SnO₂ [58], and comparable to that of 3D NiO/TiO₂ [59]. The degradation of the PCC can be related to the smooth surface and low surface area (about 5.0 m²/g) compared to the porous treated carbon cloth (CC-FeD). Such low surface area and the smooth surface leads to poor intercalation of lithium ion after continuous cycling by the PCC electrode. Furthermore, the PCC electrode exhibited slow transportation of ions and electrons that leads to poor kinetics and eventually causing low discharge capacity and degradation.

Interestingly, upon the contribution of the magnetite NPs in the CC-Fe₃O₄ electrode, the capacities of the CC-FeD electrode are still very much comparable that of the CC-Fe₃O₄ (1.66 and 0.94 mA h/cm²). It should be noted that the treated CC still maintain a high discharge capacity upon its high mass weight. For example, according to Fig. 3c, based on the mass weight of the electrodes (around 10 g/cm²), the CC-FeD exhibited a discharge capacity of 168 and 97 mA h/g at 175 and 1860 mA/g current densities, which is comparable to that of CC-Fe₃O₄ (176 and 99 mA h/g) and exceptionally higher than the PCC counterparts (35 and 5 mA h/g). Moreover, based on the capacity contribution of the CC mentioned above, it can be observed that about 94% of the capacity delivered by the CC-Fe₃O₄ electrode comes from the CC (see SI for detail evaluations), which further confirmed that the dominating active material in the CC-Fe₃O₄ electrode is the N-doped porous CC.

In order to test the effect of ultrafast charging and discharging ability of the electrodes, the discharge-charge measurements were examined at increasing current densities. Fig. 3d demonstrates the plot of decreasing capacity as a function of cycle number at various current densities. The CC-FeD electrode delivered a discharge capacity of 0.66 mA h/cm² at a current density of 3720 mA/g, which is 52% of its initial capacity at 175 mA/g. Such rate capacity is

almost equal to that of the CC-Fe₃O₄ at 0.68 mA h/cm² (48% of its initial capacity at 1.41 mA h/cm²) and 44 fold higher than the PCC (18% of its initial capacity at 0.82 mA h/cm²). A capacity up to 1.28 mA h/cm² (99% of its initial capacity) was still recorded as the current density reduces to 175 mA/g. This is indicative of excellent reversibility and high stability and higher than the PCC electrode and 3D carbon array [60]. Same as in the case of the cyclic stability for the capacity based on the weight of the electrodes, when cycled up to 3720 mA/g, the CC-FeD electrode could retain a capacity of 78 mA h/g. Understandings about the electrochemical insight of the electrodes were further studied by electrochemical impedance spectroscopy (EIS). The equivalent circuit for fittings of the EIS data is displayed in Fig. S12a. The Nyquist plots of the PCC, CC-Fe₃O₄ and CC-FeD electrodes are shown in Fig. 3e. The impedances of both CC-Fe₃O₄ and CC-FeD electrodes are almost the same, which are significantly lower than that of the PCC. This indicates that the treated CC exhibit better kinetics and possesses good electrical conductivity over the PCC electrode. Furthermore, the impedance of the CC-FeD electrode obviously decreases after cycling according to the EIS result (Fig. S12b). Additionally, the SEM images collected from the electrodes after cycling displayed that the porous morphology of the CC-FeD electrode can still be well recognized (Fig. S13a-b), likewise the Fe₃O₄ NPs still rigidly adheres to the inner part of the CC (Fig. S13c-d). These results confirmed that the N-doped porous carbon cloth electrodes exhibited excellent structural stability.

3.4. Lithium storage properties of the CC-LCO Cathode

To demonstrate all-flexible based LIBs, we employed commercially available LCO casted on the flexible CC-FeD substrate as cathode (denoted as CC-LCO) (See Experimental section for details preparation). In this case, our as-fabricated N-doped porous CC-FeD stands as a flexible substrate for the casting of LCO. The mass loading is about 2.0 mg/cm². Our strategy to improve the flexible properties of LIBs is to assemble full FLIB with highly flexible and mechanically stable anode and cathode. Unlike many reported works and our previous works that often utilizes the Al coated LCO as cathode, the use of coating cathode material on high mechanically stable conductive substrate might be effective in improving the flexible features of LIBs. Firstly, we study the morphology, crystallographic phase and lithium storage properties of the CC-LCO sample. SEM images of the CC-LCO show that the LCO NPs are uniformly casted on the CC (Fig. 4a and b). XRD pattern shows the presence of both LCO and CC (Fig. 4c). The charge/discharge profiles of the CC-LCO are displayed in Fig. 4d. According to this curves, the CC-LCO cathode could achieved an initial charge and discharge capacities of 0.28 mA h/cm² (161 mA h/g) and 0.23 mA h/cm² (143 mA h/g). These values are relatively higher than the theoretical capacity of commercial LCO. Further electrochemical performance of the CC-LCO is displayed in Fig. 4e. The CC-LCO electrode achieved a discharge capacity of 0.22 mA h/cm² (107 mA h/g) at 100 mA/g after 10 cycles, and decreases to 0.14 mA h/cm² (71 mA h/g) at 2000 mA/g. When run for another 100 cycles after rate capability test, capacity retention of 94% can be retained. The excellent performance of the CC-LCO cathode can be attributed to the N-doped 3D porous CC-FeD flexible substrate with mechanical supports, which enable easy transportation of ions and electrons in the CC-LCO. EIS data collected for the electrode after electrochemical reactions in Fig. 4f shows that its impedance is smaller than the electrode impedance before electrochemical processes. This suggested improves in kinetics of the CC-LCO cathode.

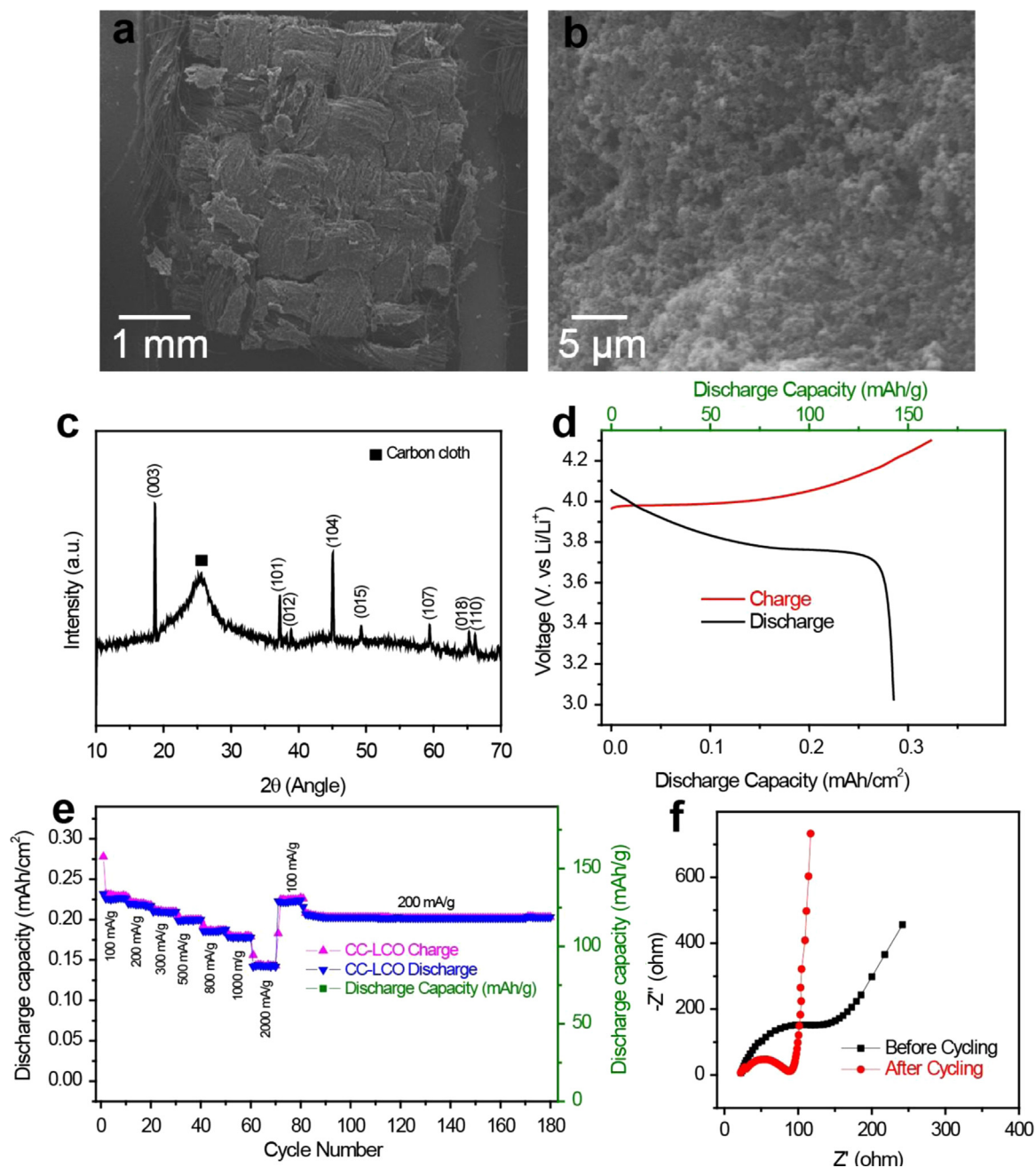


Fig. 4. Properties of the CC-LCO sample. (a and b) SEM images and (c) XRD pattern. (d) Charge/discharge curves and (e) rate and cyclic performance. (f) Nyquist plot of the electrode before and after cycling.

4. All-flexible lithium ion batteries

For the full cell electrochemical studies, the CC-FeD anode and CC-LCO cathode (CC-FeD//CC-LCO) were assembled in both coin-cell and flexible configuration. In the coin cell configuration, the coin cell was assembled by using 0.25 cm² CC-FeD anode and 1.0 cm² CC-LCO cathode since the capacity delivered by the CC-FeD is almost 5 times that of the CC-LCO in the half-cell storage. In the same vein, full coin cell LIB consisting of PCC anode and CC-LCO cathode (PCC//CC-LCO) was also assembled for comparison. Both CC-FeD//CC-LCO and PCC//CC-LCO full cells both recorded a working voltage of 3.4 V, with discharge capacities of 0.25 and 0.17 mA h/cm², respectively at a current of 0.125 mA/cm² (Fig. S14). To justify the excellent performance of the CC-FeD//CC-LCO device over the PCC//CC-LCO, cyclic stability test was performed at

a current density of 1.0 mA/cm² for 200 cycles (Fig. 5a). The cyclic performance of the CC-FeD//CC-LCO and CC-FeD//CC-LCO LIBs shows that the CC-FeD//CC-LCO exhibited attractive cyclic stability delivering a capacity of 0.137 mA h/cm² (equivalent to 87% of its initial capacity), which is higher than the PCC//CC-LCO cell at 0.068 mA h/cm² (57% capacity retention). This indicated that the CC-FeD electrode also presents better lithium storage than the PCC electrode in the full cell configuration.

To demonstrate the flexibility of the all-flexible CC-FeD//CC-LCO device, series of experiment was carried out for the device at the different bending positions. The sizes of the electrode materials were scaled-up to 6.0 cm² and the steps in assembling the flexible cell are shown in Fig. S15. The schematic diagram illustrating the assembling of the flexible LIB device is depicted in Fig. 5b. The Nyquist plots of the flexible device at different

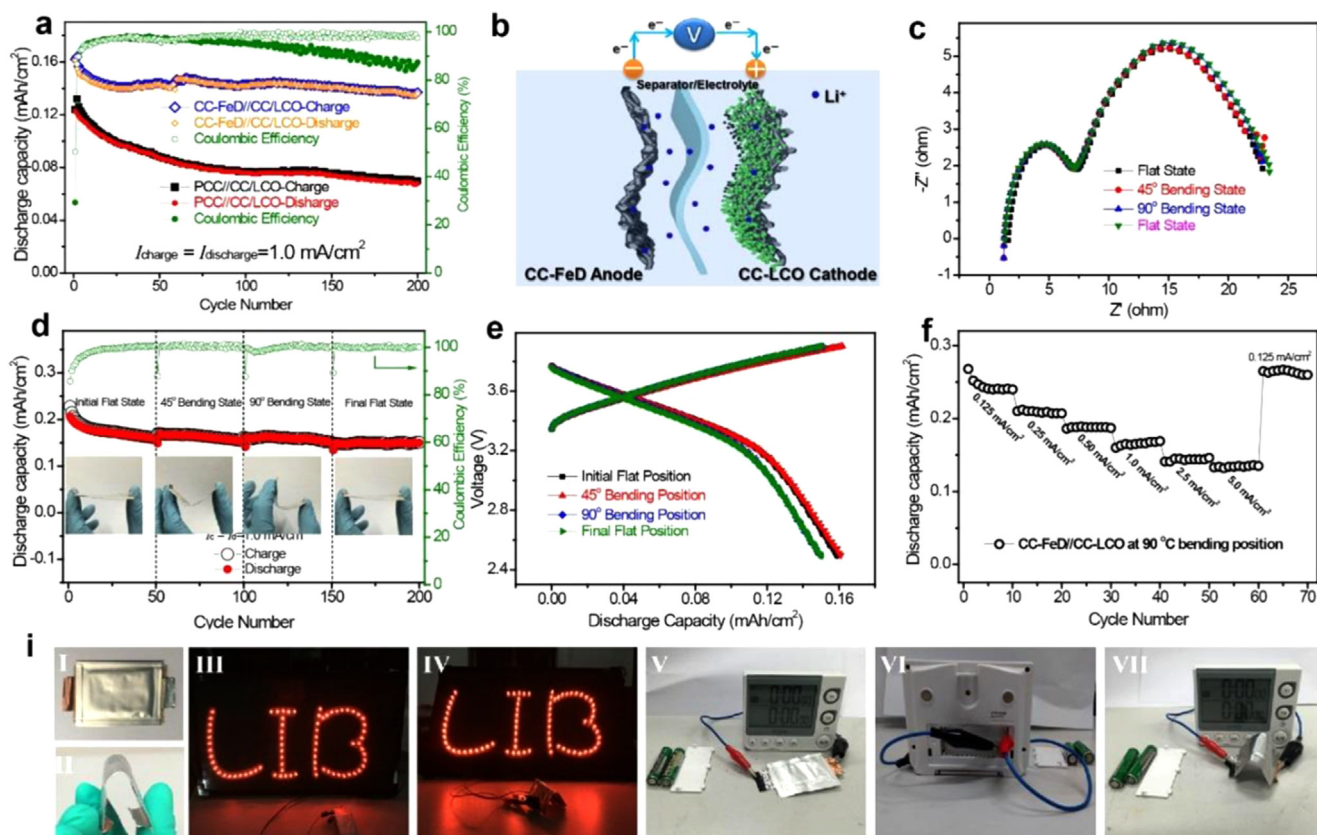


Fig. 5. Electrochemical Performance of the full coin cell and all-flexible LIB devices. (a) Cyclic stability of the PCC//CC-LCO and CC-FeD//CC-LCO coin cell LIB at a current density of 1.0 mA/cm^2 . (b) Schematic illustration of the CC-FeD//CC-LCO all-flexible LIB device. (c) Nyquist plots, (d) cyclic stability at a current density of 1.0 mA/cm^2 and (e) charge-discharge curves of the CC-FeD//CC-LCO all-flexible LIB device at the flat, 45° and 90° bending position. (f) Rate capability of the PCC//CC-LCO and CC-FeD//CC-LCO coin cell LIB. (i) Optical images of the CC-FeD//CC-LCO all-flexible LIB (I and II) used in lightening “LIB plate” (III and IV) and a “stopwatch” (V–VII) in the flat and bending positions, respectively.

positions are very similar indicating that the flexibility and bendability have little or no effect on the resistance of the device (Fig. 5c). The CC-FeD//CC-LCO FLIB device was tested for 50 cycles each at different bending conditions and 1.0 mA/cm^2 current density. The digital images of the corresponding bending angles are displayed in Fig. 5d inset. The device displayed discharge capacities of 0.159 , 0.160 and 0.150 mA h/cm^2 at the flat, 45° and 90° bending position, respectively (Fig. 5d). When the device was returned to the flat position and tested for another 50 cycles, the flexible LIB device could retained 95% its initial capacity after long and rigorous cycling at the different bending positions. Even at different bending conditions at the end of each cycling, the voltage/capacity plots looks very identical indicating that the flexibility has less effect on the voltage variations (Fig. 5e).

Finally, rate capability test was carried out for the all-flexible device at 90° bending angle. The CC-FeD//CC-LCO also showed a remarkable rate-performance exhibiting a capacity of 0.136 mA h/cm^2 up to 5.0 mA/cm^2 current density (Fig. 5f). This shows that the CC-FeD//CC-LCO device interpreted better flexibility. This can be attributed to the excellent flexibility of both electrodes in the all flexible CC-FeD//CC-LCO device. It should be pointed out that the capacity of the full flexible cell (0.150 mA h/cm^2) and full coin cell (0.155 mA h/cm^2) are almost the same at the same testing conditions, demonstrating that scaling up to large size and flexibility shows little or no influence on our all-flexible LIB device. The flexible CC-FeD//CC-LCO device could deliver a maximum volumetric energy density of 43 W h/cm^3 at 0.125 mA/cm^2 and volumetric power density 800 W/cm^3 at 5.0 mA/cm^2 . After electrochemical processes, our

CC-FeD//CC-LCO all-flexible LIB device (Fig. 5i–II) could drive a “LIB light-emitting-diodes (LED) plate” (Fig. 5i–III, IV) and stop-watch device (Fig. 5i–V–VII) at the flat and bending positions, respectively (Fig. 5i). The all-flexible battery was used to control stop-watch device (Video 1) as demonstrated in (Fig. 5i–V–VII). All these results indicate that our strategy of employing the flexible cathode is suitable for the development of flexible LIBs.

Supplementary material related to this article can be found online at [doi:10.1016/j.nanoen.2016.05.017](https://doi.org/10.1016/j.nanoen.2016.05.017).

Finally, to justify that our strategy to enhanced the lithium storage performance of commercial CC is general, repeatable, effective and efficient, we extended the same method to improve the electrochemical performance of CC through thermal reduction of other metal transition metal oxide precursors such as cobalt oxide precursor. The product obtained is named CC-CoD. The CC-CoD anode also displayed better electrochemical performance than the CC. Detail results about the morphology, characterization and excellent electrochemical performance of the CC-CoD sample can be seen in Fig. S16. The excellent performance of the N-doped porous carbon cloth can be attributed to (i) the N heteroatom doping N doping of the CC, which could enhances the electrochemical reactivity, electronic conductivity and kinetics, and attractively contributes to the remarkable capacity achieved by the porous CC samples [61,62] and (ii) the porous surface leading to large surface area that is significant for providing rich sites for electrode/electrolyte interface to absorb Li ions and rapid electron transfer.

5. Conclusions

In conclusion, we have successfully demonstrated an effective and easily repeatable strategy to utilize the low capacity commercial carbon cloth as electrode material for LIBs through hydrothermal, thermal reduction and acid treatment. With respect to thermal reduction of the metal oxides and acid-treatment, the carbon cloth (CC-FeD and CC-CoD) became porous, which leads to considerable increase surface area. Additionally, the surfaces of the carbon cloth were functionalized with N-heteroatoms, which could further enhance the electrochemical activity and electrical conductivity of the carbon cloth. When tested as anode material for LIBs, the N-doped porous CC-FeD exhibited excellent lithium storage ability with attractive capacity, remarkable rate capability and stable cyclic stability over the PCC. Moreover, a flexible LIB based on our as-prepared CC-FeD anode and CC-LCO cathode (CC-FeD//CC-LCO) was assembled. The N-doped porous CC-FeD was used as flexible substrate for the LCO coating. The CC-FeD//CC-LCO flexible LIB possesses a high working voltage of 3.4 V, outstanding lithium storage performance and excellent flexibility over the Al coated based flexible device. These work open the chance of developing more flexible high-performance electrode materials for energy storage based on our modified CC strategy.

Acknowledgements

This work was supported by the National Natural Science Foundation of China (21273290, 21476271 and 51521001), the Natural Science Foundation of Guangdong Province (S2013030013474 and 2014KTSCX004) and the Science and Technology Plan Project of Guangdong Province (2014B101123002, 2014B050505001 and 2015B010118002).

Appendix A. Supporting information

Supplementary data associated with this article can be found in the online version at <http://dx.doi.org/10.1016/j.nanoen.2016.05.017>.

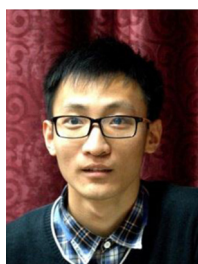
References

- [1] Y. Gogotsi, *Nature* 509 (2014) 568–570.
- [2] A.M. Gaikwad, B.V. Khau, G. Davies, B. Hertzberg, D.A. Steingart, A.C. Arias, *Adv. Energy Mater.* 5 (2015) 1401389.
- [3] B. Liu, J. Zhang, X. Wang, G. Chen, D. Chen, C. Zhou, G. Shen, *Nano Lett.* 12 (2012) 3005–3011.
- [4] X. Pu, L. Li, H. Song, C. Du, Z. Zhao, C. Jiang, G. Cao, W. Hu, Z.L. Wang, *Adv. Mater.* 27 (2015) 2472–2478.
- [5] D. Akinwande, N. Petrone, J. Hone, *Nat. Commun.* 5 (2014) 5678–5689.
- [6] H. Chen, S. Zeng, M. Chen, Y. Zhang, Q. Li, *Carbon* 92 (2015) 271–296.
- [7] X. Lu, M. Yu, G. Wang, Y. Tong, Y. Li, *Energy Environ. Sci.* 7 (2014) 2160–2181.
- [8] G. Zhou, F. Li, H.-M. Cheng, *Energy Environ. Sci.* 7 (2014) 1307–1338.
- [9] B.C. Kim, J.-Y. Hong, G.G. Wallace, H.S. Park, *Adv. Energy Mater.* 5 (2015) 1500959.
- [10] L. Hu, H. Wu, F. La Mantia, Y. Yang, Y. Cui, *ACS Nano* 4 (2010) 5843–5848.
- [11] X. Wang, X. Lu, B. Liu, D. Chen, Y. Tong, G. Shen, *Adv. Mater.* 26 (2014) 4763–4782.
- [12] M.F. De Volder, S.H. Tawfik, R.H. Baughman, A.J. Hart, *Science* 339 (2013) 535–539.
- [13] Y. Zhang, W. Bai, X. Cheng, J. Ren, W. Weng, P. Chen, X. Fang, Z. Zhang, H. Peng, *Angew. Chem. Int. Ed.* 53 (2014) 14564–14568.
- [14] N. Li, Z. Chen, W. Ren, F. Li, H.-M. Cheng, *P. Natl. Acad. Sci. USA* 109 (2012) 17360–17365.
- [15] S. Wang, B. Pei, X. Zhao, R.A. Dryfe, *Nano Energy* 2 (2013) 530–536.
- [16] L. Shen, Q. Che, H. Li, X. Zhang, *Adv. Funct. Mater.* 24 (2014) 2630–2637.
- [17] Y.-Z. Zhang, Y. Wang, T. Cheng, W.-Y. Lai, H. Pang, W. Huang, *Chem. Soc. Rev.* 44 (2015) 5181.
- [18] J.-X. Feng, Q. Li, X.-F. Lu, Y.-X. Tong, G.-R. Li, *J. Mater. Chem. A* 2 (2014) 2985–2992.
- [19] M.-S. Balogun, C. Li, Y. Zeng, M. Yu, Q. Wu, M. Wu, X. Lu, Y. Tong, *J. Power Sources* 272 (2014) 946–953.
- [20] M.-Q. Zhao, C.E. Ren, Z. Ling, M.R. Lukatskaya, C. Zhang, K.L. Van Aken, M. W. Barsoum, Y. Gogotsi, *Adv. Mater.* 27 (2015) 339–345.
- [21] S. Liu, Z. Wang, C. Yu, H.B. Wu, G. Wang, Q. Dong, J. Qiu, A. Eychmüller, *Adv. Mater.* 25 (2013) 3462–3467.
- [22] J.X. Feng, S.H. Ye, A.L. Wang, X.F. Lu, Y.X. Tong, G.R. Li, *Adv. Funct. Mater.* 24 (2014) 7093–7101.
- [23] M.-S. Balogun, M. Yu, Y. Huang, C. Li, P. Fang, Y. Liu, X. Lu, Y. Tong, *Nano Energy* 11 (2015) 348–355.
- [24] M.-S. Balogun, M. Yu, C. Li, T. Zhai, Y. Liu, X. Lu, Y. Tong, *J. Mater. Chem. A* 2 (2014) 10825–10829.
- [25] S.-Y. Lee, K.-H. Choi, W.-S. Choi, Y.H. Kwon, H.-R. Jung, H.-C. Shin, J.Y. Kim, *Energy Environ. Sci.* 6 (2013) 2414–2423.
- [26] C. Guan, X. Wang, Q. Zhang, Z. Fan, H. Zhang, H.J. Fan, *Nano Lett.* 14 (2014) 4852–4858.
- [27] J. Zhu, K. Sakaushi, G. Clavel, M. Shalom, M. Antonietti, T.-P. Fellingner, *J. Am. Chem. Soc.* 137 (2015) 5480–5485.
- [28] T. Liu, L. Finn, M. Yu, H. Wang, T. Zhai, X. Lu, Y. Tong, Y. Li, *Nano Lett.* 14 (2014) 2522–2527.
- [29] X.-F. Lu, X.-Y. Chen, W. Zhou, Y.-X. Tong, G.-R. Li, *ACS Appl. Mater. Interfaces* 7 (2015) 14843–14850.
- [30] P. Yang, Y. Ding, Z. Lin, Z. Chen, Y. Li, P. Qiang, M. Ebrahimi, W. Mai, C.P. Wong, Z.L. Wang, *Nano Lett.* 14 (2014) 731–736.
- [31] X. Lu, T. Liu, T. Zhai, G. Wang, M. Yu, S. Xie, Y. Ling, C. Liang, Y. Tong, Y. Li, *Adv. Energy Mater.* 4 (2014) 1300994–1301000.
- [32] C. Wang, W. Wan, Y. Huang, J. Chen, H.H. Zhou, X.X. Zhang, *Nanoscale* 6 (2014) 5351–5358.
- [33] G. Zhang, S. Hou, H. Zhang, W. Zeng, F. Yan, C.C. Li, H. Duan, *Adv. Mater.* 27 (2015) 2400–2405.
- [34] W. Song, X. Hou, X. Wang, B. Liu, D. Chen, G. Shen, *Energy Technol.* 2 (2014) 370–375.
- [35] W. Li, Z. Yang, Y. Jiang, Z. Yu, L. Gu, Y. Yu, *Carbon* 78 (2014) 455–462.
- [36] S. Komaba, W. Murata, T. Ishikawa, N. Yabuuchi, T. Ozeki, T. Nakayama, A. Ogata, K. Gotoh, K. Fujiwara, *Adv. Funct. Mater.* 21 (2011) 3859–3867.
- [37] Y.-S. Chen, Y. Li, H.-C. Wang, M.-J. Yang, *Carbon* 45 (2007) 357–363.
- [38] C. Hu, Y. Xiao, Y. Zhao, N. Chen, Z. Zhang, M. Cao, L. Qu, *Nanoscale* 5 (2013) 2726–2733.
- [39] R. Zou, Z. Zhang, M.F. Yuen, M. Sun, J. Hu, C.-S. Lee, W. Zhang, *NPG Asia Mater.* 7 (2015) e195–e202.
- [40] G. Wang, H. Wang, X. Lu, Y. Ling, M. Yu, T. Zhai, Y. Tong, Y. Li, *Adv. Mater.* 26 (2014) 2676–2682.
- [41] W. Wang, W. Liu, Y. Zeng, Y. Han, M. Yu, X. Lu, Y. Tong, *Adv. Mater.* 27 (2015) 3572–3579.
- [42] K. Jost, C.R. Perez, J.K. McDonough, V. Presser, M. Heon, G. Dion, Y. Gogotsi, *Energy Environ. Sci.* 4 (2011) 5060–5067.
- [43] Q.-Q. Xiong, J.-P. Tu, X.-H. Xia, X.-Y. Zhao, C.-D. Gu, X.-L. Wang, *Nanoscale* 5 (2013) 7906–7912.
- [44] Y. Luo, J. Luo, J. Jiang, W. Zhou, H. Yang, X. Qi, H. Zhang, H.J. Fan, Y. Denis, C. M. Li, *Energy Environ. Sci.* 5 (2012) 6559–6566.
- [45] X. Lu, Y. Zeng, M. Yu, T. Zhai, C. Liang, S. Xie, M.S. Balogun, Y. Tong, *Adv. Mater.* 26 (2014) 3148–3155.
- [46] Y. Luo, M.-S. Balogun, W. Qiu, R. Zhao, P. Liu, Y. Tong, *Chem. Commun.* 51 (2015) 13016–13019.
- [47] Y. Zeng, Y. Han, Y. Zhao, Y. Zeng, M. Yu, Y. Liu, H. Tang, Y. Tong, X. Lu, *Adv. Energy Mater.* 5 (2015) 1402176–1402182.
- [48] M.-S. Balogun, Z. Wu, Y. Luo, W. Qiu, X. Fan, B. Long, M. Huang, P. Liu, Y. Tong, *J. Power Sources* 308 (2016) 7–17.
- [49] X.-Y. Yu, H. Hu, Y. Wang, H. Chen, X.W. Lou, *Angew. Chem. Int. Ed.* 54 (2015) 7395–7398.
- [50] D. Li, C. Lv, L. Liu, Y. Xia, X. She, S. Guo, D. Yang, *ACS Cent. Sci.* 1 (2015) 261–269.
- [51] Y. Chen, X. Li, K. Park, J. Song, J. Hong, L. Zhou, Y.-W. Mai, H. Huang, J. B. Goodenough, *J. Am. Chem. Soc.* 135 (2013) 16280–16283.
- [52] Z.-S. Wu, W. Ren, L. Xu, F. Li, H.-M. Cheng, *ACS Nano* 5 (2011) 5463–5471.
- [53] L. Qie, W.M. Chen, Z.H. Wang, Q.G. Shao, X. Li, L.X. Yuan, X.L. Hu, W.X. Zhang, Y. H. Huang, *Adv. Mater.* 24 (2012) 2047–2050.
- [54] J. Ni, Y. Huang, L. Gao, *J. Power Sources* 223 (2013) 306–311.
- [55] V.G. Khomenko, V.Z. Barsukov, *Electrochim. Acta* 52 (2007) 2829–2840.
- [56] W. Wang, M. Tian, A. Abdulgatov, S.M. George, Y.-C. Lee, R. Yang, *Nano Lett.* 12 (2012) 655–660.
- [57] W. Zeng, F. Zheng, R. Li, Y. Zhan, Y. Li, J. Liu, *Nanoscale* 4 (2012) 2760–2765.
- [58] G.F. Ortiz, I. Hanzu, P. Lavela, P. Knauth, J.L. Tirado, T. Djenizian, *Chem. Mater.* 22 (2010) 1926–1932.
- [59] M.-S. Balogun, W. Qiu, Y. Luo, Y. Huang, H. Yang, M. Li, M. Yu, C. Liang, P. Fang, P. Liu, Y. Tong, *ChemElectroChem* 2 (2015) 1243–1248.
- [60] H.-S. Min, B.Y. Park, L. Taherabadi, C. Wang, Y. Yeh, R. Zaouk, M.J. Madou, B. Dunn, *J. Power Sources* 178 (2008) 795–800.

- [61] X. Liu, D. Chao, Y. Li, J. Hao, X. Liu, J. Zhao, J. Lin, H. Jin Fan, Z. Xiang Shen, *Nano Energy* 17 (2015) 43–51.
- [62] M.-S. Balogun, Z. Wu, Y. Luo, W. Qiu, X. Fan, B. Long, M. Huang, P. Liu, Y. Tong, *J. Power Sources* 308 (2016) 7–17.



Muhammad-Sadeeq Balogun is currently a final year Physical Chemistry Doctorate candidate in the School of Chemistry and Chemical Engineering, Sun Yat-Sen University through the Chinese Scholarship Council. His principal investigator is Prof. Yexiang Tong. He obtained his bachelor degree in industrial chemistry from Olabisi Onabanjo University, Nigeria in 2008. He received his Masters degree in Materials Chemistry in 2012 at Guilin University of Electronic Technology, China under the supervision of Prof. Zhongmin Wang. His current research focuses on the development of nanomaterials and their applications in lithium ion batteries, sodium ion batteries and water splitting.



Feiyi Lyu is currently an undergraduate student in chemistry at Sun Yat-Sen University and will graduate June 2016. His research focuses on the synthesis and characterization of electrode materials for Li-ion batteries application.



Yang Luo received his bachelor degree in the major of Materials Science and Engineering, Tianjin Polytechnic University. He was a visiting student at the Wuhan University in July and August in 2014. Currently, he is an M. Sc. student in the School of Chemistry and Chemical Engineering, Sun Yat-Sen University. His research interests mainly focus on lithium ion and sodium ion batteries and their working mechanism.



Weitao Qiu received his BS degree in chemistry from Sun Yat-Sen University in 2014. He is currently a 2nd year master of physics and chemistry student in Prof. Yexiang Tong's group at Sun Yat-Sen University. His research focuses on the development of nanostructured materials for the application of Li-ion batteries and photoelectrochemical water splitting.



Hui Meng received his PhD degree in material physics and chemistry from Sun Yat-sen University(2006). Then he worked in INRS-EMT, Canada and BNL, United States. He is now associate professor in Jinan University. His research focuses in the application of electrochemistry in energy devices such as fuel cells, lithium ion/air batteries and supercapacitors.



Jiantao Li received his BS degree in Materials Science and Engineering from Wuhan University of Technology in 2013. He is currently a 3rd year PhD candidate and doing research in Prof. Liqiang Mai's group. His research mainly focuses on electrochemical energy storage & conversion materials, especially in the fields of supercapacitors and electrochemical water splitting.



Wenjie Mai received his B. S. degree in Physics (2002) from Peking University (PKU) and his Ph.D. degree in Materials Science and Engineering (2009) from the Georgia Institute of Technology (GIT). He is now a Professor in Jinan University (JNU). His main research interest includes energy conversion, harvesting and storage devices, such as supercapacitors, dye-sensitised solar cells, nanogenerators, and photoelectrochemical water splitting.



Liqiang Mai is Chair Professor of Materials Science and Engineering at Wuhan University of Technology (WUT). He received his Ph.D. from WUT in 2004. He carried out his postdoctoral research in the laboratory of Prof. Zhonglin Wang at Georgia Institute of Technology in 2006–2007 and worked as advanced research scholar in the laboratory of Prof. Charles M. Lieber at Harvard University in 2008–2011. His current research interests focus on nanowire materials and devices for energy storage. He received the National Natural Science Fund for Distinguished Young Scholars, the First Prize for Hubei Natural Science Award and so forth. He was selected as National Hundred-Thousand-Ten Thousand Project Leading Talent and granted the honorary title of "Young and Middle-aged Experts with Outstanding Contributions" of China.



Yexiang Tong is currently a professor in School of Chemistry and Chemical Engineering at Sun Yat-Sen University, PR China. Prof. Yexiang Tong received his BS in General Chemistry in 1985, MS in Physical Chemistry in 1988, and PhD in Organic Chemistry in 1999 from Sun Yat-Sen University. He joined Sun Yat-Sen University as an Assistant Professor of Chemistry in 1988. His current research focuses on the electrochemical synthesis of alloys, intermetallic compounds and metal oxide nanomaterials, and investigation of their applications for energy conversion and storage.